In vivo and simultaneous multimodal imaging: Integrated multiplex coherent anti-Stokes Raman scattering and two-photon microscopy

Dong Li, Wei Zheng, Yan Zeng, and Jianan Y. Qu[a)]
Department of Electronic and Computer Engineering, Hong Kong University of Science and Technology, Clear Water Bay, Kowloon, Hong Kong

(Received 20 September 2010; accepted 5 November 2010; published online 29 November 2010)

Simultaneous multimodal imaging is critical for *in vivo* study of biological dynamic processes and clinical applications. In this study, we demonstrate a multimodal nonlinear optical (NLO) microscopy of the capability to simultaneously produce images of multiplex coherent anti-Stokes Raman scattering (M-CARS), two-photon excitation fluorescence, and second harmonic generation in living biological systems. The excitation sources are a femtosecond Ti:sapphire laser and a broadband supercontinuum generated from a photonic crystal fiber. The simultaneously excited multiple NLO signals were recorded by using a time- and wavelength-resolved detection technique. In M-CARS imaging, the nonresonant background is effectively reduced by using a simple background subtraction method. © *2010 American Institute of Physics*. [doi:10.1063/1.3521415]

In past two decades, nonlinear optical (NLO) microscopy technology has been significantly developed and its applications in biological research have been widely explored.[1] Recently, the multimodal NLO microscopy techniques have been reported as a powerful tool to characterize the biological systems.[2–6] For coherent anti-stokes Raman scattering (CARS) microscopy, the picosecond sources of narrow spectral bandwidth have been commonly used to reduce the nonresonant background (NRB). However, the reduced excitation efficiency of picosecond laser hinders its applications to other NLO imaging, such as second harmonic generation (SHG) and two-photon excitation fluorescence (TPEF), especially for the weak intrinsic fluorescence. In previous studies, the CARS and TPEF signals were either excited sequentially by switching between picosecond and femtosecond excitation sources[2,3] or excited simultaneously by using the femtosecond sources but leave the NRB unprocessed.[4,5] A dual pump CARS has been introduced to subtract the NRB by using a picosecond pump laser and two optical parametric oscillators as the excitation sources.[7] The recently developed frequency modulation CARS also subtracts the NRB based on the same principle.[8] In this work, we develop an integrated multimodal NLO microscopy to produce multiplex CARS (M-CARS), TPEF, and SHG of living biological samples simultaneously. In particular, the excitation source consists of a Ti:sapphire laser supplemented with a photonic crystal fiber (PCF)-based supercontinuum generator to perform the M-CARS measurements. A simple subtraction procedure is used to reduce the NRB signals in CARS.[7,8]

The schematic of the home-built multimodality NLO microscopy is shown in Fig. 1. Briefly, a femtosecond Ti:sapphire laser (Chameleon Ultra II, Coherent, Santa Clara, CA) tuned at 780 nm was used to pump a PCF (NL-1.4-775, NKT photonics, Birkerød, Denmark). The near infrared (NIR) supercontinuum was selected by using a long pass (LP) filter as the Stokes light of CARS excitation. A portion of the femtosecond laser was used as the pump light for CARS signals and the excitation of TPEF and SGH signals. A laser line filter (LL01-780, Semrock, Rochester, NY) was used to narrow the bandwidth of the pump light down to 65 cm^{-1} to match the bandwidth of aliphatic C–H stretch and improve the spectral resolution of the M-CARS. In order to optimize the temporal overlapping between the pump and broadband NIR supercontinuum light, we compensated the positive group delay dispersion introduced by the PCF and the optics of the imaging system by using two prism-based compressors. The pulse duration of the pump and supercontinuum light at focal point, measured with an autocorrelator (Pulse Check-50, APE, Berlin, Germany), were about 400 and 250 fs, respectively. After compression, the pump and NIR supercontinuum light were combined by a dichroic mirror (900DCXR, Chroma, Bellows Falls, VT) and directed collinearly through a dichroic mirror. A Zeiss C-Apochromat uv-vis-ir objective (40×, numerical aperture 1.2, water im-

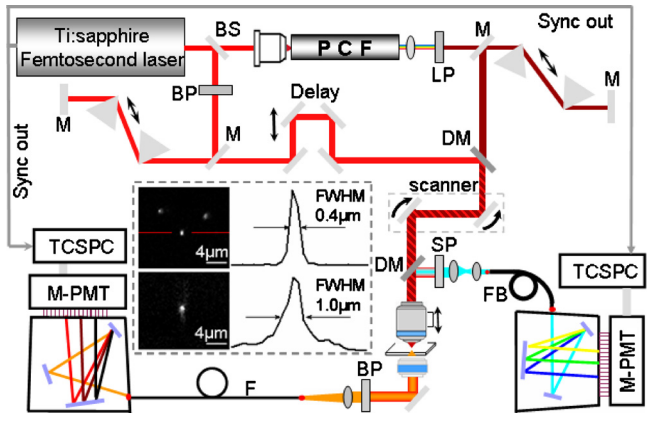

FIG. 1. (Color online) Schematic of the multimodal NLO microscopy. BS: beam splitter; M: mirror; BP: band pass filter; LP: long pass filter; DM1: dichroic mirror (900 DCXRU); DM2: dichroic mirror (600 DCXRU); SP: short pass filter; F: single fiber; FB: fiber bundle, M-PMT: multichannel PMT. Inset: CARS images of 0.2 μm diameter polystyrene beads measured in horizontal plane (upper panel) and vertical plane (lower panel) for the measurements of lateral and axial resolutions. The intensity profiles along the line indicated in the figure show the lateral and axial resolution are about 0.4 and 1.0 μm, respectively.

[a)]Present address: Department of Electronic and Computer Engineering, Hong Kong University of Science and Technology, Clear Water Bay, Kowloon, Hong Kong. Tel.: (852) 2358-8541. FAX: (852) 2358-1485. Electronic mail: eequ@ust.hk.

mersion) was used to focus the excitation light to the sample and collect the backscattered NLO signals. The dichroic mirror reflected TPEF and SHG signals to a custom designed fiber bundle that conducted the signals to a spectrograph equipped with a multichannel photomultiplier tube (PMT) and a time correlated single photon counting (TCSPC) module (PML-16-C-0 and SPC-150, Becker and Hickl, Berlin, Germany). The detection system recorded the time-resolved signals from 380 to 580 nm with 13 nm resolution. The forward CARS (F-CARS) signals were collected by a condenser (U-LWCD, Olympus, Tokyo, Japan) and focused into a fiber. The F-CARS signals were recorded by second multichannel TCSPC system (PML-16-C-1 and SPC-150, Becker and Hickl) covering the wavelength range from 600 to 700 nm. The total power incident on the samples was about 25 mW and the acquisition time was 8 s for each optical sectioning depth.

The M-CARS measurements, covering the vibrational frequency from 2200 to 3400 cm^{-1}, detect the pure NRB and the CARS signals of aliphatic C–H and water O–H bonds at the same time. It is noted that in the high wavenumber region the effective vibrational band widths of the aliphatic C–H and water O–H band are large, ~130 and ~400 cm^{-1}, respectively. Therefore, it is expected that the broadband excitations of femtosecond laser and supercontinuum will not suffer the excitation efficiency of CARS signals and compromise the CARS contrast.[4,5] However, the challenge is to effectively reduce the NRB signals that are composed of the additive term and mixing term proportional to $(\chi_{NR}^{(3)})^2$ and $\chi_{NR}^{(3)} \cdot \mathrm{Re}(\chi_R^{(3)})$, respectively.[9] Here $\chi_R^{(3)}$ is the resonant and $\chi_{NR}^{(3)}$ is the nonresonant third order nonlinear susceptibility. Because the mixing NRB term signals are determined by both $\chi_R^{(3)}$ and $\chi_{NR}^{(3)}$, they only appear with the resonant scatters in the CARS image. On the contrary, the additive NRB signals could occur throughout the whole image. As shown in the results later, the spatial distribution of additive NRB signals is not necessarily uniform and cannot be simply removed by using a background offsetting. In this study, we develop a simple procedure to subtract the additive NRB from the CARS image.

Though CARS signal and additive NRB mix with each other in the vibrationally resonant wavelength region, the nonresonant signal is theoretically independent on the wavelength and the additive NRB in the vibrationally resonant region could be calculated from the signal measured in the pure nonresonant region.[7] In principle, the NRB signal in the vibrationally resonant region (I_{NR}) and in nonresonant region (I'_{NR}) can be measured from a completely nonresonant sample, such as a glass coverslip to generate a calibration ratio of I_{NR}/I'_{NR} for every pixel. A typical pure nonresonant spectrum measured from a glass coverslip using our multimodal NLO imaging system is shown in Fig. 2(a). We generated the calibration ratios via dividing the signal ($I_{NR\text{-}CH}$) in the aliphatic C–H bond region from 2650 to 2970 cm^{-1} and the signal ($I_{NR\text{-}OH}$) in the water O–H bond region from 2970 to 3380 cm^{-1} by the signal (I'_{NR}) in nonresonant region from 2200 to 2650 cm^{-1}, respectively. When measuring a biological sample, the additive NRBs in C–H bond and O–H bond vibrational regions were calculated by multiplying the ratios ($I_{NR\text{-}CH}/I'_{NR}$ and $I_{NR\text{-}OH}/I'_{NR}$) with the nonresonant signal measured from 2200 to 2650 cm^{-1}, respectively. The NRBs were then subtracted from the total signals measured

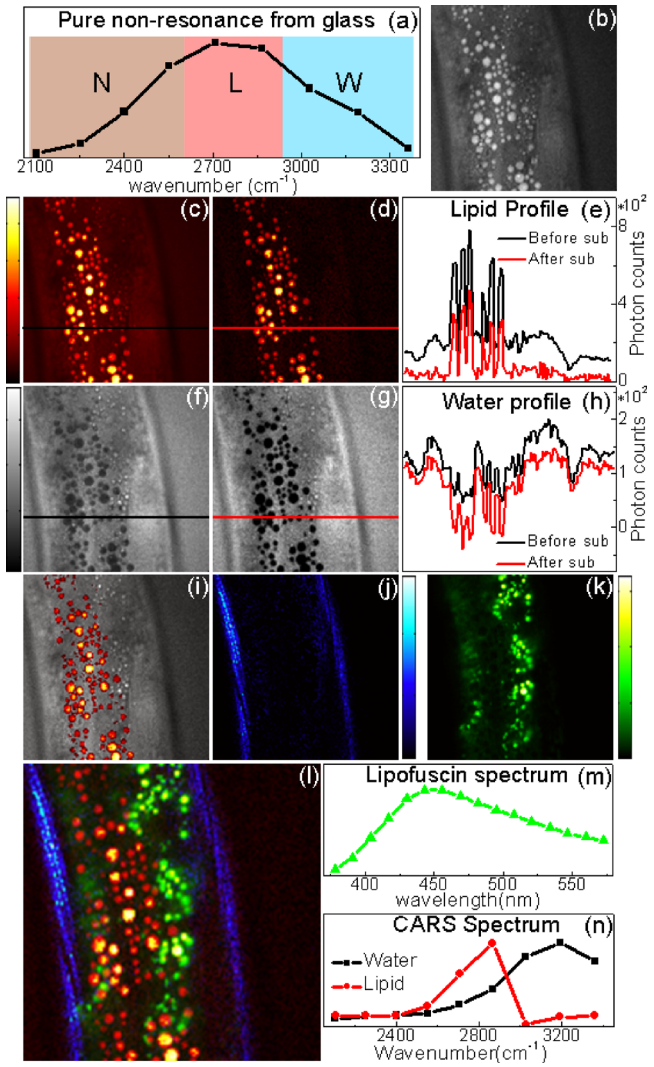

FIG. 2. (Color online) Representative multimodal NLO images of living *C.elegans*. (a) Pure nonresonant spectrum measured from a glass coverslip. N: nonresonance vibrational band; L: aliphatic C–H vibrational band; W: water O–H vibrational band; (b) pure nonresonant image measured from *C.elegans*; (c) aliphatic C–H bond CARS image before NRB subtraction; (d) after NRB subtraction; (e) intensity profile of C–H bond CARS signals; (f) water O–H bond CARS image before NRB subtraction; (g) after NRB subtraction; (h) intensity profile of O–H bond CARS signals; (i) subtracted features in gray scale and residual lipid droplets colored in red; (j) SHG image; (k) TPEF image; (l) merged image; (m) TPEF spectrum of lipofuscin granules; (n) the CARS spectra of lipid droplets and water content after NRB subtraction.

in the vibrationally resonant regions. Moreover, the calibration ratio also took into account the spectral nonuniformity of the broadband Stokes light and the response differences between 16-wavelength detection channels.

The representative multimodal NLO images of *C.elegans* are shown in the Fig. 2. All images were acquired simultaneously from the same sampling area of 90×90 um. The pure NRB image measured from *C.elegans* that integrated the signals from 2200 to 2650 cm^{-1} is shown in Fig. 2(b). As can be seen, significant NRB signals were measured from lipid droplets and bulk water content inside the body of *C.elegans* and from the surrounding agar gel. The distribution of NRB signals is obviously nonuniform across the whole image, indicating that a simple offsetting will not be able to remove the NRB accurately and the NRB must be subtracted based on the calibration ratio calculated pixel by

pixel. The CARS images of aliphatic C–H and water O–H bonds, which map the lipid and water distribution, before NRB subtraction are shown in Figs. 2(c) and 2(f), respectively. The corresponding images after NRB subtraction are shown in Figs. 2(d) and 2(g), respectively. The NRB signals arising from the bulk medium were obviously reduced by the subtraction method. For a quantitative comparison, the intensity profiles along the lines indicated in corresponding images before and after NRB subtraction are displayed in Figs. 2(e) and 2(h), respectively. As shown in Fig. 2(e), after NRB subtraction the CARS signals of C–H bond almost dropped to zero in the water rich regions of *C.elegans* and surrounding agar gel. In contrast, the CARS signals of O–H bond reach the minimum in the neutral lipid droplets region as shown in Fig. 2(h). The results demonstrate that the additive NRB signals were effectively reduced. In particular, the gray-scaled image of the subtracted features in Fig. 2(i) shows large number of small sized lipid dropletlike features (bright spots) contributed from additive NRB were effectively subtracted. This indicates the importance of NRB subtraction to differentiate the true resonant CARS features from false features in CARS imaging. As shown in Figs. 2(f) and 2(g), these dropletlike features appeared in O–H bond CARS images. This further confirms that they are not lipid droplet, but associated with water or molecular clusters of strong O–H bond.

The SHG and TPEF images excited by the pump light are displayed in Figs. 2(i) and 2(j), respectively. The backscattered SHG signals from the myosin filaments in the muscle fibers were clearly isolated from the strong TPEF signals at the channel of half pump light wavelength as shown in Fig. 2(i). The TPEF image in Fig. 2(j) shows bright spots of strong fluorescence emission in the body of *C.elegans*. Previous studies identified that the origins of the bright spots are lipofuscin granules, the secondary lysosomes.[10] The C-H bond CARS, lipofuscin TPEF, and muscle SHG images were merged together as shown in Fig. 2(l). Comparing the merged image with the O–H bond CARS image in Fig. 2(g), we found that neutral lipid droplets must be hydrophobic because no water signals were measured from the droplets. The water signals and lipofuscin granules mixed up well with each other, indicating that the lipofuscin granules are hydrophilic and formed from different species of lipids.[11] Fluorescence spectrum and lifetime are two kinds of important characteristics of a fluorophore. Our multimodal NLO microscopy allows simultaneously acquiring them. The fluorescence spectrum of lipofuscin granules shown in Fig. 2(m) was measured using image-guided analysis method.[12] The emission spectrum of lipofuscin is peaked around 450 nm at 780 nm excitation. Furthermore, the average fluorescence lifetime of lipofuscin granules is around 0.6 ns. Similarly, the CARS spectra of lipid droplets and water rich region were obtained and shown in Fig. 2(n). The CARS spectra of lipid droplets and water are peaked around 2850 and 3200 cm^{-1}, respectively. The negative dip in the CARS spectrum of lipid is due to the dispersive characteristics of the real part of the third order susceptibility.[9]

In conclusion, the integrated M-CARS module and two-photon excitation microscopy has been demonstrated. The NLO images of CARS, TPEF, and SHG are acquired simultaneously. The NRB could be significantly reduced by a simple background subtraction. The time- and spectral-resolved detection capability is critical to collect and extract accurate information from the multimodal NLO signals. The M-CARS images provide important information on lipid and water contents/distributions in living biological system. The system could be easily modified to image the thick tissue samples whose epi-detected CARS signals are enhanced by the backscattering of the forward propagating F-CARS photons.

This work is supported by the Hong Kong Research Grants Council through Grant No. HKUST618808.

[1] B. R. Masters and P. T. C. So, *Handbook of Biomedical Nonlinear Optics* (Oxford, New York, 2008).
[2] T. T. Le, C. W. Rehrer, T. B. Huff, M. B. Nichols, I. G. Camarillo, and J. X. Cheng, J. Biomed. Opt. **12**, 054007 (2007).
[3] F. Lu, W. Zheng, J. Lin, and Z. Huang, Appl. Phys. Lett. **96**, 133701 (2010).
[4] A. F. Pegoraro, A. Ridsdale, D. J. Moffatt, Y. Jia, J. P. Pezacki, and A. Stolow, Opt. Express **17**, 2984 (2009).
[5] H. Chen, H. Wang, M. N. Slipchenko, Y. Jung, Y. Shi, J. Zhu, K. K. Buhman, and J. X. Cheng, Opt. Express **17**, 1282 (2009).
[6] R. S. Lim, A. Kratzer, N. P. Barry, S. M. Anzai, M. Miyazaki, W. W. Mantulin, M. Levi, E. O. Potma, and B. J. Tromberg, J. Lipid Res. **51**, 1729 (2010).
[7] O. Burkacky, A. Zumbusch, C. Brackmann, and A. Enejder, Opt. Lett. **31**, 3656 (2006).
[8] F. Ganikhanov, C. L. Evans, B. G. Saar, and X. S. Xie, Opt. Lett. **31**, 1872 (2006).
[9] C. L. Evans and X. S. Xie, Annu. Rev. Anal. Chem. **1**, 883 (2008).
[10] G. V. Clokey and L. A. Jacobson, Mech. Ageing Dev. **35**, 79 (1986).
[11] T. T. Le, H. M. Duren, M. N. Slipchenko, C. D. Hu, and J. X. Cheng, J. Lipid Res. **51**, 672 (2010).
[12] D. Li, W. Zheng, and J. Y. Qu, Opt. Lett. **33**, 2365 (2008).